*Acta Cryst.* (1970). A26, 128

# Dispersion of Piezo-optic Constants of Some Alkali Halides in the Ultraviolet Region. I. Determination of Absolute Values

BY A. RAHMAN AND K. S. IYENGAR

*Department of Physics, Osmania University, Hyderabad-7, India*

(*Received* 8 *April* 1969)

Static and ultrasonic methods are described for the determination of the piezo-optic coefficients, $q_{11}-q_{12}$ and $q_{44}$, and the strain-optic ratios, $p_{12}/p_{11}$ and $(p_{11}+p_{12}-2p_{44})/(p_{11}+p_{12}+2p_{44})$, for NaCl, KCl, KBr and KI. Dispersion of the absolute elasto-optical constants, $p_{11}$, $p_{12}$ and $p_{44}$ is evaluated. Comparison is made with predictions of Bansigir & Iyengar's theory of the piezo-optic effect in cubic crystals. The occurrence of isotropy of birefrigence for uniaxial stress and uniaxial strain at different wavelengths of light is explained.

## Introduction

The dispersion of piezo-optic birefringence in cubic crystals was originally reported by Iyengar (1955) for three wavelengths of light in the visible region. Subsequently Bansigir & Iyengar (1958) employing an improved technique studied the variation of birefringence in the alkali halides NaCl, KCl and KBr in the wavelength range 4800–6000 Å. The investigations confirmed the existence of a measurable dispersion amounting to 5–10%. Srinivasan (1959) carried the investigations into the ultraviolet region and observed large variations for NaCl, KCl, KBr and KI in the vicinity of the fundamental absorption band. He also reported sign reversals of birefringence in potassium halides. This property of enhanced induced birefringence close to an absorption band now appears to be universal, as has been demonstrated in semiconducting materials (ZnO, CdS, Tell, Warlock & Martin, 1965; GaAs, Si, Nikitenko & Martynenko, 1965; ZnSe, Dubenskii, Kaplyanskii & Lozovskaya, 1967). The studies of Srinivasan (1959) were confined to the variation of the differential piezo-optic coefficient $q_{11}-q_{12}$ which measures the birefringence produced when the crystal is stressed in the direction of a cube axis and observations are made along a different axis. Similar variations of the coefficient $q_{44}$ (stress along a face diagonal and observation along a cube axis) have been reported by Rahman & Iyengar (1967). Recently Laiho & Korpela (1968) have extended this study to rubidium and cesium halides.

The evaluation of the individual coefficients $q_{11}$ and $q_{12}$ and the corresponding elasto-optic coefficients, $p_{11}$ and $p_{12}$, are of considerable theoretical interest (Bansigir & Iyengar 1961). Other aspects of interest from the band structure point of view will be discussed in part II. The discussion in this part of the paper will be confined to a description of the experimental method followed for the evaluation of the coefficients and the results obtained therefrom.

## Static method

### *Determination of $q_{11}-q_{12}$ and $q_{44}$*

The method of Bansigir & Iyengar (1958) modified to apply to the ultraviolet region has been followed. The optical arrangement is shown schematically in Fig. 1. A hydrogen discharge lamp, $H$, illuminates a small aperture, $O_1$, through the condensing lens, $L_1$. The lens $L_2$ (followed by a Wollaston double-image prism, $P$) forms an image of the aperture $O_1$ close to the fused silica block, $S$. The aperture $O_2$ allows only one of the two beams produced by the double-image prism to pass through the block $S$, the crystal, $C$, and the second Wollaston prism, $A$. Lens $L_3$ then forms an image of the aperture $O_2$ on the slit of a quartz spectrograph $Sp$. The second beam produced by the double image prism $A$ is not allowed to enter the spectrograph. The orientation of the double-image prisms is such that the beams allowed to reach $Sp$ from both prisms, are polarized at an angle of 45° to the vertical.

The fused silica block and the crystal are stressed by the use of an arrangement of levers. A crystal block with edges parallel to the [110], [1$\bar{1}$0] and [001] direc-

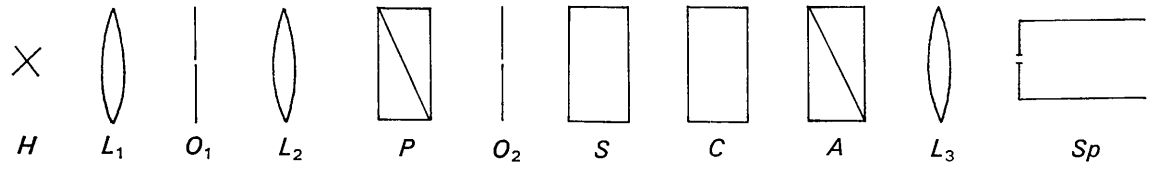


Fig. 1. Optical arrangement for the static method. $H$, hydrogen discharge lamp; $O_1$ and $O_2$, small apertures; $L_1$, condensing lens; $L_2$ and $L_3$, fused silica lenses; $P$ and $A$, Wollaston double image prisms; $S$, fused silica block; $C$, crystal; $Sp$, quartz spectrograph.

tions is used for determining $q_{44}$. The stress is applied parallel to [110] and light propagation is along [001]. For measuring the coefficient $q_{11}-q_{12}$, edges of the crystal block are parallel to the cube axis and observation is along another axis.

When either the silica block or the crystal, or both, are stressed, the continuous spectrum in *Sp* is crossed with dark bands. The position of a band at wavelength $\lambda$ Å is given by:

$$R = n \,.\, \lambda/2 \,, \tag{1}$$

where $R$ is the total relative retardation for light polarized parallel and perpendicular to the stress direction, due to passage through the stressed material, and $n$ is an odd integer. Measurements were made on the bands corresponding to $n=3$ and 5 because these are quite sharp for the values of $R$ encountered in these investigations.

The spectrograph *Sp* was calibrated with a low pressure mercury arc. In the continuous spectrum of the hydrogen discharge, the line $H_\beta$, which is easily identified, serves as a point of reference for measuring the wavelength corresponding to the centre of a band, using a comparator.

The dispersion of the differential stress-optic coefficient, $C_1$, of the fused silica specimen was determined first by applying various loads and locating the band position. The retardation is given by

$$R = C_1 P_1 t \,, \tag{2}$$

where $P_1$ is the stress on the silica block and $t$ the length of the light path within it. From (1) and (2) $C_1$ is evaluated. A series of spectra for various loads on the silica block is shown in Fig. 2.

Two procedures were followed to evaluate the differential stress-optical coefficient of the crystal, taking into account the small residual birefringence which the crystals exhibited. In one procedure a band due to the passage of light through both stressed silica block and the unstressed crystal is observed at, say, $\lambda_0$ Å near the visible region. The total relative retardation is then

$$R_1 + R_2^0 = n\lambda_0/2 \,, \tag{3}$$

where $R_1$ is the relative retardation in the stressed silica block and $R_2^0$ that due to residual birefringence in the crystal. $R_1$ is found from equation (2) for the wavelength $\lambda_0$ and hence $R_2^0$ is determined. A set of spectra are now recorded, keeping a constant stress $P_2$ on the crystal and varying the stress on the silica block. From this set one spectrum is chosen which has a band at $\lambda'$ Å close to $\lambda_0$. For this band

$$R_1 + R_2 + R_2^0 = n\lambda'/2 \,, \tag{4}$$

where $R_1$ and $R_2$ are relative retardations due to the applied stress in the silica block and the crystal respectively, and $R_2^0$ is that due to residual birefringence in the crystal. Since $\lambda_0$ and $\lambda'$ are close and the dispersion of birefringence in the visible range is small, one can use the value of $R_2^0$ from (3) in (4) and finally evaluate $R_2$. The differential stress-optical coefficient of the crystal $C_2$ for that wavelength is given by

$$R_2 = C_2 P_2 t_2 \,, \tag{5}$$

where $P_2$ is the stress on the crystal specimen and $t_2$ the length of the light path in it. Knowing $C_2$ one can find the value of the residual stress from

$$R_2^0 = C_2 P_2^0 t_2 \,. \tag{6}$$

Using the rest of the spectra one can find the differential stress-optical coefficient $C_2$ for other wavelengths. For a band at $\lambda$ Å we have

$$R_1 + R_2' = n\lambda/2 \,. \tag{7}$$

$R_1$, the relative retardation in the silica block, is found in the manner described above and thus $R_2'$, the total relative retardation in the crystal, is known. From the relation

$$R_2' = C_2(P_2 + P_2^0)t_2 \,, \tag{8}$$

$C_2$ can now be evaluated.

In the second procedure, three sets of spectra are recorded. For each set the stress on the crystal is kept fixed and the load on the silica block varied, so shifting the bands to different regions of the spectrum. From each set the relative retardation due to the stressed crystal is found corresponding to the band positions, and relative retardation *versus* wavelength curves are plotted. From the three curves thus obtained, each for a fixed stress on the crystal, values of relative retardation and corresponding stress are noted for selected wavelengths and for each of these a relative retardation *versus* stress curve is drawn. We find a linear relation between stress and relative retardation for the range of stresses used in these experiments. These lines have a common intercept on the stress axis, which gives the value of the residual stress. From the slopes of these lines we find the differential stress-optic coefficient for various wavelengths. Results obtained by the two methods are found to be in good agreement. The piezo-optic constants $q_{11}-q_{12}$ and $q_{44}$ are related to the differential stress-optic coefficient, $C$, as follows:

$$(q_{11}-q_{12}) = 2/n^3 \,.\, S_{100}, \quad q_{44} = 2/n^3 \,.\, S_{110} \,, \tag{9}$$

where $n$ is the refractive index of the crystal in the undeformed state and $S_{100}$ and $S_{110}$ represent the values of the stress-optic coefficient for an applied stress parallel to [100] and [110] respectively. The strain-optic constants $p_{11}-p_{12}$ and $p_{44}$ are given by

$$p_{11}-p_{12} = (q_{11}-q_{12})\,(C_{11}-C_{12}), \quad p_{44} = q_{44} \,.\, C_{44} \tag{10}$$

where $C_{11}$, $C_{12}$ and $C_{44}$ are the elastic constants.

## Dynamic method

*Determination of* $p_{12}/p_{11}$ *and* $(p_{11}+p_{12}-2p_{44})/(p_{11}+p_{12}+2p_{44})$

The experimental arrangement is shown in Fig. 3. Light from a 400 watt Hanovia arc after passing

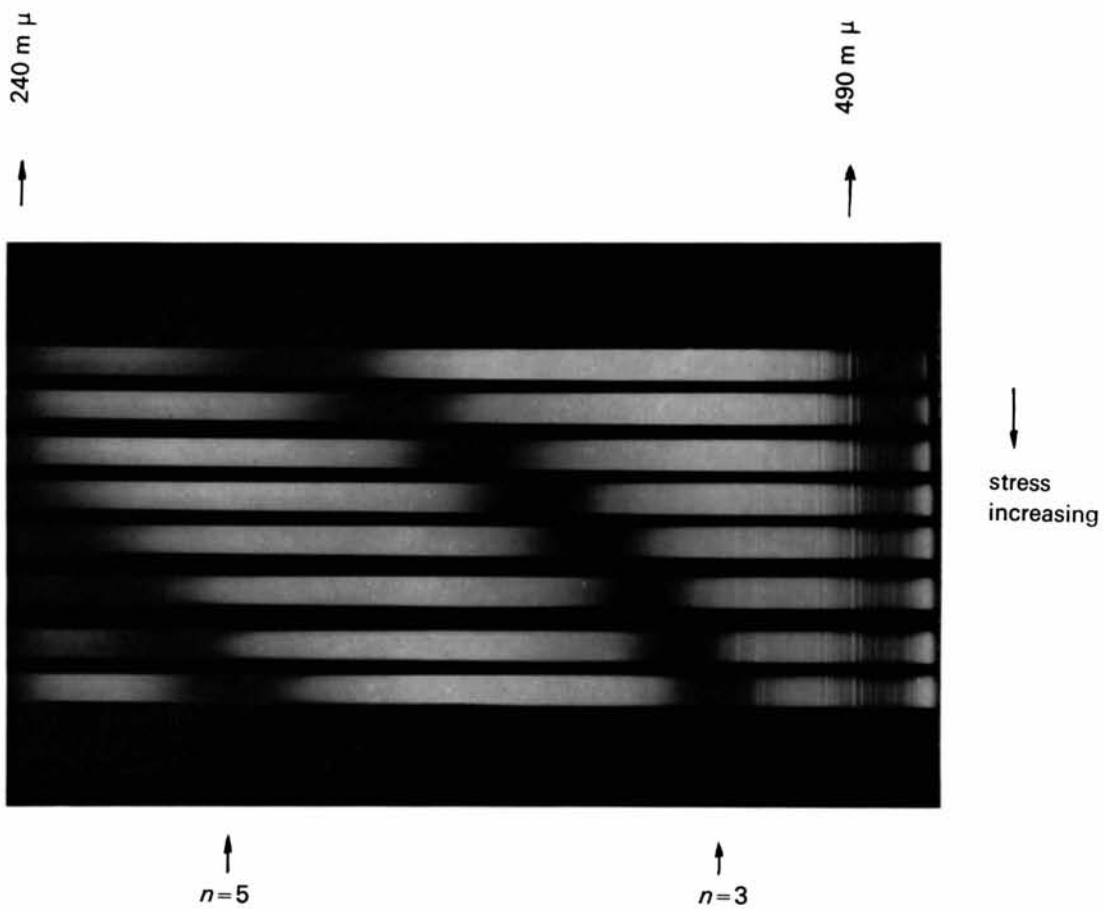


Fig. 2. Interference bands in the hydrogen spectrum due to stressed fused silica. The movement of bands of order 3 and 5 is shown for increasing stress.

[To face p. 129

through an adjustable horizontal slit $S$ is collimated by the lens $L_1$. The collimated beam then enters the crystal under investigation, $C$, a double-image prism, $D$, and finally the quartz prism, $Q$, of a medium quartz spectrograph. When the length of the slit is suitably adjusted, the prominent lines of the mercury spectrum are recorded as two sets of horizontal lines, one above the other, on the photographic plate placed at $PP$. The crystal rests on the ultrasonic transducer $T$ and when suitably excited a longitudinal standing wave is set up in it. This results in each spectral line being split up into a number of diffraction orders giving rise to the familiar Hiedemann pattern. Mueller (1938) has shown on theoretical grounds that the ratio of the intensities of the corresponding diffraction lines of the $m$th order in the two polarized sets has the value $B_m^0 = R^{2m}$, where $B_m^0$ is the limiting ratio of intensities when the sound amplitude is reduced to zero; and $R = p_{12}/p_{11}$ or $(p_{11}+p_{12}-2p_{44})/(p_{11}+p_{12}+2p_{44})$ depending on whether the direction of propagation of sound in the crystal is along [100] or [110] respectively, with the light beam travelling in a direction normal to that of sound along a cube axis.

At low levels of ultrasonic excitation only the first diffraction order is recorded and the relative intensity of the corresponding two spectral sets is determined with the help of an analyser (Polariod sheet HNP'B) interposed at $A$ (Fig. 3) following the double image prism $D$. $B_m$ is obtained from the identity $B_m = \tan^2 \alpha$, where $\alpha$ is the angle through which the analyser must be rotated in order to equalize the intensities of the corresponding spectral images. In practice this was realized by photographing the pattern for various positions of the analyser at 2° intervals and measuring the relative intensities with a microphotometer. The position of equal intensities was then determined by interpolation. This process was repeated for a few values of sound amplitude in decreasing order and the limiting ratio $B_m^0$ was then obtained. Care must be taken while using polarizer HNP'B in this type of work below

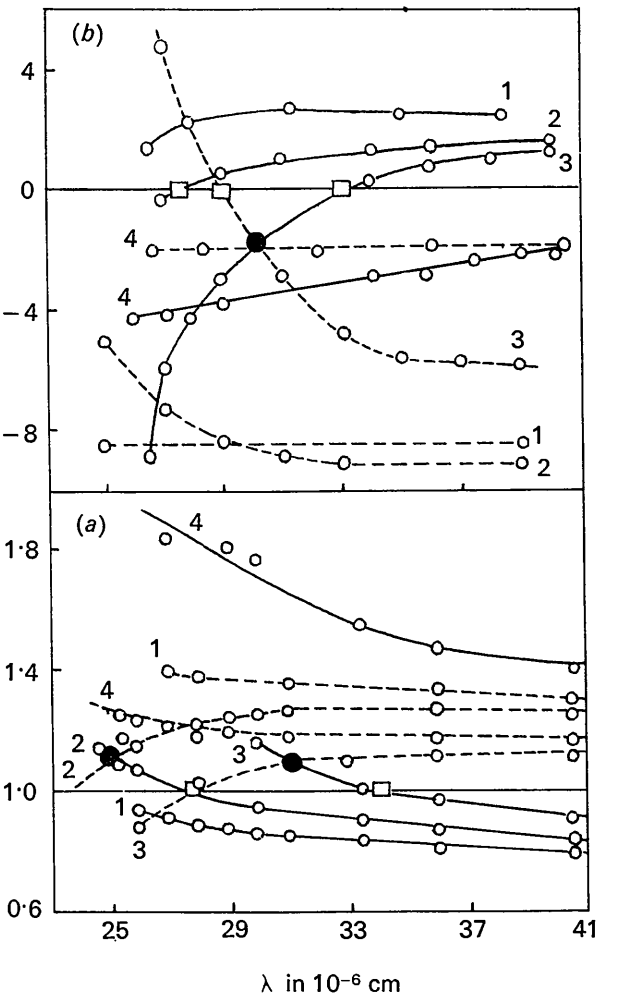


Fig. 4. Dispersion of stress-optical coefficients and strain-optical ratios. ●, isotropy; □, sign reversal of birefringence. 1, KCl; 2, KBr; 3, KI; 4, NaCl. (*a*) Strain-optical ratios: $p_{12}/p_{11}$ —○—; $(p_{11}+p_{12}-2p_{44})/(p_{11}+p_{12}+2p_{44})$ ---○---. (*b*) Stress-optical coefficients: $\frac{1}{2}n^3(q_{11}-q_{12})$ —○—; $\frac{1}{2}n^3 q_{44}$ ---○---.

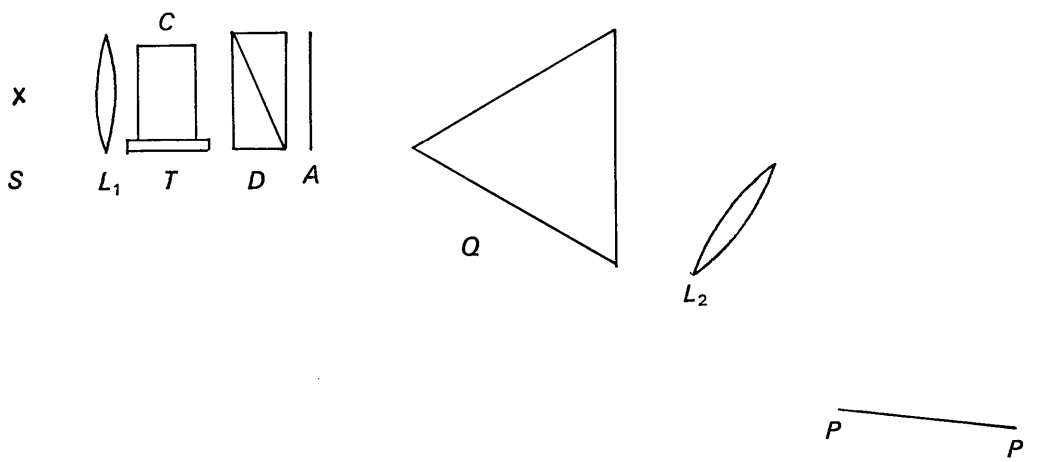


Fig. 3. Optical arrangement for the ultrasonic method. $S$, horizontal slit; $L_1$, collimator lens; $C$, crystal; $T$, transducer; $D$, double image prism; $A$, analyzer; $Q$, quartz prism; $L_2$, camera lens; $PP$, photographic plate.

$\lambda = 2800$ Å. In that region this polarizer transmits a significant portion of light polarized normal to its characteristic direction. Using the transmission curves supplied by the Polaroid Corporation, the extinction coefficients for wavelengths below 2800 Å are computed and these are used in applying corrections to observed intensity ratios.

### Preparation of crystal specimens

The crystals used in these investigations were grown from Analar material employing the Kyropoulos technique. The orientation of the crystal block was controlled to an accuracy of $\pm\frac{1}{2}°$. Immediately after polishing the specimen, 2 mm thick plane parallel fused silica plates of Spectrosil quality were pasted, with a drop of castor oil, to the polished surfaces to protect them from moisture and to improve the optical quality of the light transmitting surfaces. The fused silica block used was of Spectrosil quality.

### Results and discussion

The results of the static and dynamic methods are represented graphically in Fig. 4 in the wavelength region 2500–4100 Å. With these data the curves of Fig. 5, depicting the variations of the individual coefficients $p_{11}$, $p_{12}$ and $p_{44}$, have been evaluated. All these curves show rapid variations of the elasto-optic and the piezo-optic birefringence as the absorption band is approached. At a certain wavelength which is characteristic of each solid the stress-induced birefringence totally disappears. At this point the birefringence reverses in sign. The reversal wavelengths are given in Table 1.

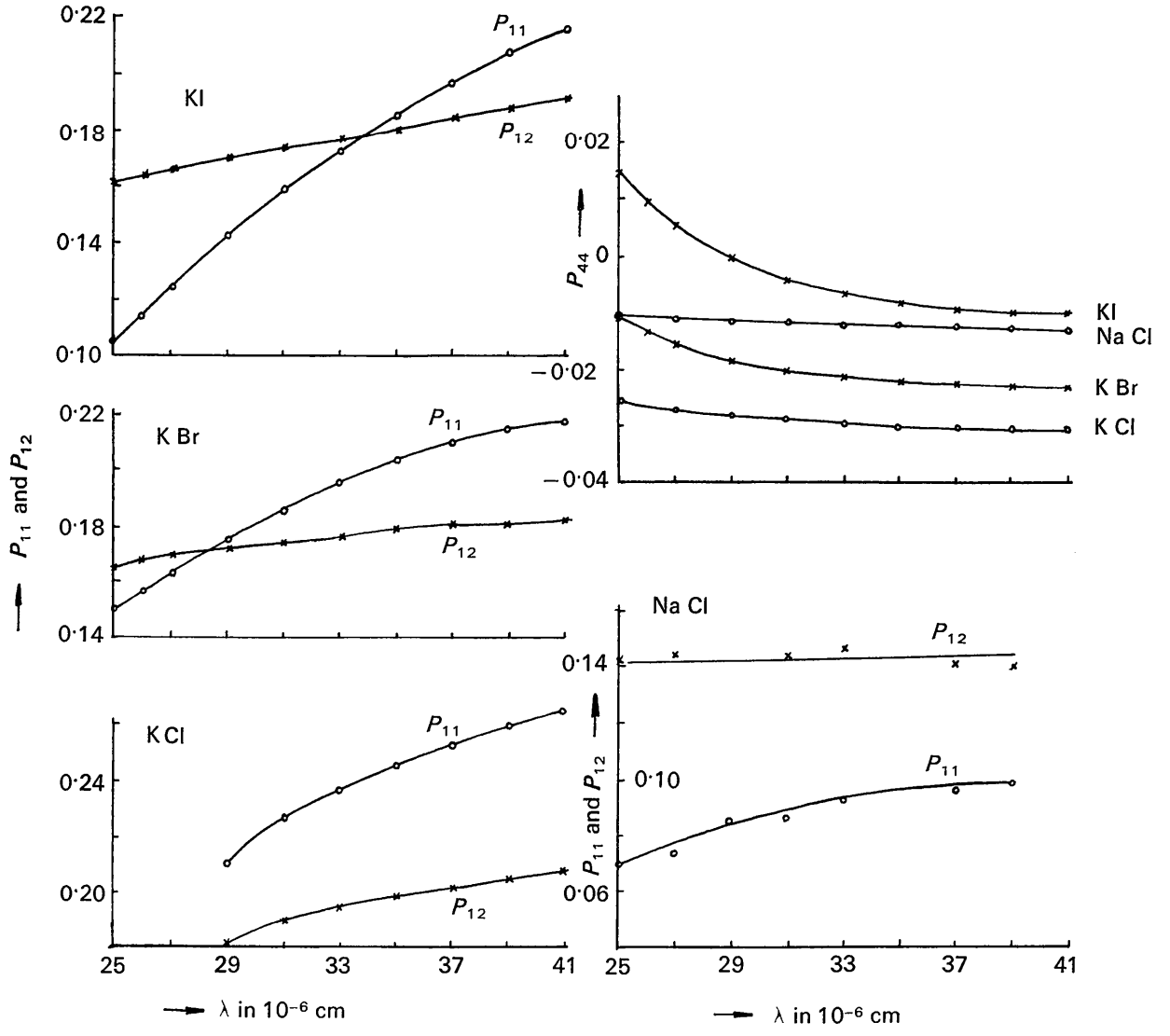


Fig. 5. Dispersion of strain-optical constants $p_{11}$, $p_{12}$ and $p_{44}$ in KCl, KBr, KI and NaCl.

Table 1. *Reversal wavelengths for the elasto-optic coefficients* $p_{11}-p_{12}$ *and* $p_{44}$

| Crystal | Reversal wavelengths in mμ | | Values at reversal |
|---|---|---|---|
| | $p_{11}-p_{12}$ | $p_{44}$ | $p_{11}=p_{12}$ |
| KI | 338 | 275 | 0·178 |
| KBr | 280 | – | 0·17 |
| KCl | 248 (extrapolated) | – | 0·12 |

Bansigir & Iyengar (1961) developed a theory of piezo-birefringence for crystals of the NaCl structure and they showed that $p_{11}$ and $p_{12}$ can be separately evaluated from a knowledge of the difference values $p_{11}-p_{12}$. Their equations are:

$$n^3/2\,.\,(p_{11}-p_{12})=3M-(1+\sigma)A$$
$$n^3/2\,.\,(p_{11}+2p_{12})=(3L-A)\,(1-2\sigma)$$

where $M=(n^2-1)^2\,(n^2+5)/45n$, $L=(n^2-1)\,(n^2+2)/6n$ and $\sigma$ is Poisson's ratio.

The parameter $A$ can be eliminated using the known values of $p_{11}-p_{12}$ and thus $p_{12}/p_{11}$ can be evaluated. Using the values of $p_{11}-p_{12}$ obtained in the present experiments, the ratios of $p_{12}/p_{11}$ at different wavelengths have been calculated. The values thus obtained for the crystals NaCl, KCl, KBr and KI are shown in Fig. 6. The agreement between the calculated and the observed ratios is very good in KCl, KBr and KI.

Pockels (see Mueller, 1935) has classified all cubic crystals into four groups depending on the signs of $p_{11}-p_{12}$ and $p_{44}$. KI belongs to the + − group in the region above $\lambda=3380$ Å. Below this wavelength KI changes to the − − group and at still lower wavelengths there is a change to the − + group. Similar changes are observed in the other potassium halides. The classification of Pockels, therefore, is no longer valid.

Under uniaxial stress isotropic solids like glass become equally birefringent for all directions of stress. The alkali halides also exhibit this isotropic behaviour for certain wavelengths of light. The necessary conditions for the occurrence of stress-optic and strain-optic isotropy are given by the relations

$$q_{11}-q_{12}=q_{44} \text{ and } p_{11}-p_{12}=2p_{44} \qquad (11)$$

respectively. The points of isotropy have been indicated in Fig. 4 and the wavelengths at which these occur are given in Table 2.

Equations (10) and (11) lead to the following expression in terms of the anisotropy factors:

$$(p_{11}-p_{12})/2p_{44}=(C_{11}-C_{12})/2C_{44}\,.\,(q_{11}-q_{12})/q_{44}\,. \qquad (12)$$

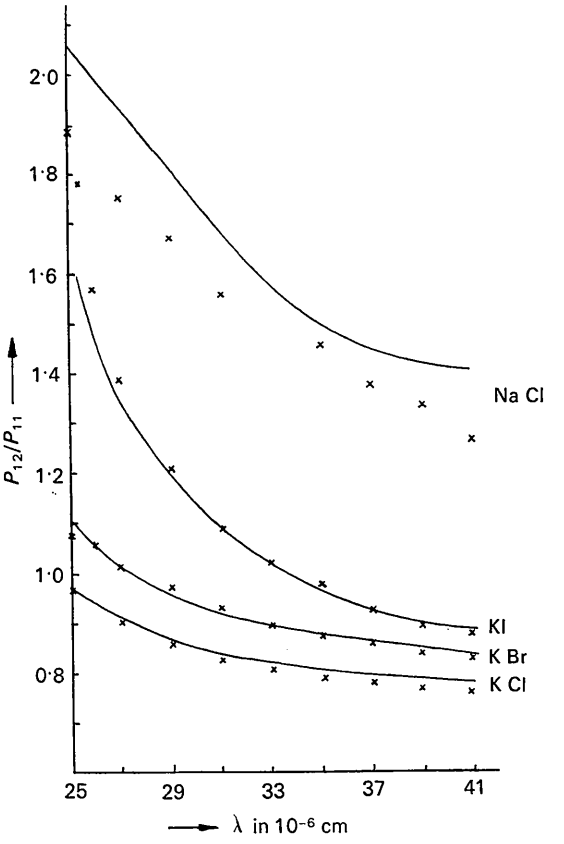


Fig. 6. Dispersion of $p_{12}/p_{11}$, observed (full curve) and calculated (×) from Bansigir & Iyengar's theory.

Since the elastic anisotropy factor $(C_{11}-C_{12})/2C_{44}$ is not generally unity for cubic crystals, the strain-optic and stress-optic conditions for isotropy are not fulfilled for the same wavelength of light. The values of the elastic anisotropy factor [calculated from the data of Spangenberg & Haussühl (1957)] and equation (12) are used together with one observed elasto-optical coefficient ($R_{100}$ or $S_{100}$) to evaluate the other coefficient ($R_{110}$ or $S_{110}$). $R_{100}$ is $p_{12}/p_{11}$ and $R_{110}$ is $(p_{11}+p_{12}-2p_{44})/(p_{11}+p_{12}+2p_{44})$. The results are shown in Table 2. For KI and NaCl, the known value of $R_{100}$ is used with the anisotropy factor and equation (12) to find $R_{110}$. For KBr, the value of $S_{100}$ is similarly used to evaluate $S_{110}$. There is general agreement between the calculated and observed values of $R_{110}$ and $S_{110}$.

Table 2. *Wavelengths of stress-optic and strain-optic isotropy*

| Crystal | Wavelength of isotropy (mμ) | $\frac{(C_{11}-C_{12})}{2C_{44}}$ | Elasto-optic coefficient | Calculated value | Observed value |
|---|---|---|---|---|---|
| KI | 302 (stress-optic) | 3·04 | $R_{110}$ | 1·05 | 1·08 |
| KBr | 250 (strain-optic) | 2·83 | $S_{110}$ | −4·56 | −5·3 |
| NaCl | 410 (stress-optic) | 1·42 | $R_{110}$ | 1·28 | 1·17 |

### References

BANSIGIR, K. G. & IYENGAR, K. S. (1958). *Proc. Phys. Soc. London*, **71**, 225.
BANSIGIR, K. G. & IYENGAR, K. S. (1961). *Acta Cryst.* **14**, 727.
DUBENSKII, K. K., KAPLYANSKII, A. A. & LOZOVSKAYA, N. G. (1967). *Sov. Phys. – Solid State* (USA), **8**, 1644.
IYENGAR, K. S. (1955). *Nature, Lond.* **176**, 1119.
LAIHO, R. & KORPELA, A. (1968). *Ann. Acad. Sci. Fenn.* A, **6**, 272.
MUELLER, H. (1935). *Phys. Rev.* **47**, 947.
MUELLER, H. (1938). *Z. Kristallogr.* A, **99**, 122.
NIKITENKO, V. I. & MARTYNENKO, G. P. (1965). *Sov. Phys. – Solid State* (USA), **7**, 494.
RAHMAN, A. & IYENGAR, K. S. (1967). *Phys. Letters*, A**25**, 478.
SPANGENBERG, K. & HAUSSÜHL, S. (1957). *Z. Kristallogr.* **109**, 422.
SRINIVASAN, R. (1959). *Z. Phys.* **155**, 281.
TELL, B., WORLOCK, J. M. & MARTIN, R. J. (1965). *Appl. Phys. Letters*, **6**, 123.


*Acta Cryst.* (1970). A**26**, 133

# Absorption Coefficients for Al 111 Systematics: Theory and Comparison with Experiment

BY P. A. DOYLE

*School of Physics, University of Melbourne, Parkville, Victoria* 3052, *Australia*

(*Received* 7 *March* 1969)

Simple physical models are taken to calculate thermal and electronic contributions to absorption coefficients in Al. *N*-beam systematic calculations are interpreted by means of 2-beam theory, making possible a comparison with the experimental values of Watanabe. The mean absorption coefficient agrees to within 25 per cent. Spherical aberration and thermal diffuse scattering within the objective aperture are shown to explain the poorer agreement for the anomalous absorption coefficient. It is concluded that weak beams are significant in the measurement of absorption coefficients. Weak systematic beams are shown to have a significant effect on the positions of the thickness fringe maxima. A brief comparison of 2- and *N*-beam rocking curves is given.

## Introduction

The theoretical interpretation of absorption coefficients in electron diffraction has been considered by several authors, but has been incomplete. Many-beam calculations including absorption have been reported for example by Howie & Whelan (1960) for Al and by Goodman & Lehmpfuhl (1967) for MgO. However, they compared experiment with arbitrary models for the absorbing potential $V_g^i$, such as $V_g^i \propto V_g^r$. On the other hand, Meyer (1966) compared absorption coefficients for Si calculated on physical models with experimental values, by mean of 2-beam theory. In the present paper, many-beam calculations are combined with absorption coefficients based on physical models of the inelastic processes for Al. The theoretical values can then be compared with those measured from elastic Bragg beams by Watanabe (1964, 1966), and the importance of weak beams studied. Detailed attention is paid to systematic errors in the experiments which tend to increase the apparent values of the mean absorption coefficient and particularly of the anomalous absorption coefficients.

## Calculation of absorption coefficients for Al

The principal contributions to inelastic scattering in Al come from phonon, plasmon and single electron excitations. The absorption coefficients due to each of these processes are calculated in this section, using approximate theories to describe each process.

### (*a*) *Thermal diffuse scattering*

Hall & Hirsh (1965) gave expressions for the mean and anomalous absorption coefficients due to thermal diffuse scattering, $\mu_0^{\mathrm{TDS}}$ and $\mu_g^{\mathrm{TDS}}$ respectively, using an Einstein model to describe the lattice vibrations. They found

$$\mu_0^{\mathrm{TDS}} = \frac{2\pi\lambda^2}{\Omega}\int f^2(\mathbf{s})\,[1-\exp(-2M_s)]s\,ds \qquad (1)$$

and

$$\mu_g^{\mathrm{TDS}} = \frac{\lambda^2}{\Omega}\iint f(\mathbf{s})f(\mathbf{s}-\mathbf{g})\,[\exp(-M_g) - \exp(-\{M_s+M_{s\text{-}g}\})]s\,ds\,d\varphi \qquad (2)$$

where the scattering vector $\mathbf{s}$ lies on the Ewald sphere, and $s = \dfrac{2\sin\theta}{\lambda}$ for a scattering angle $2\theta$. The usual Debye–Waller factor is $\exp(-M_s)$, and $\Omega$ is the unit-cell volume.

Equations (1) and (2) were derived by treating the incident wave as a Bloch wave, using 2-beam theory, and the thermal diffuse waves as plane. However, Pogany (1968) has shown that the same results for $\mu_0^{\mathrm{TDS}}$, and $\mu_g^{\mathrm{TDS}}$ for all reflexions $g$, are obtained if the